14th International Symposium on Turbulence and Shear Flow Phenomena (TSFP14)
Heidelberg, Germany, July 28–31, 2026

FREQUENCY-DEPENDENT SPECTRAL STRUCTURES IN ACTIVE GRID TURBULENCE

Nathaniel C. Durand
Mechanical and Aerospace Engineering
University of Houston
Houston, TX, 77204, United States
ncdurand@cougarnet.uh.edu

Hossein Motalebi
Mechanical and Aerospace Engineering
University of Houston
Houston, TX, 77204, United States
smotaleb@cougarnet.uh.edu

Clayton P. Byers
Department of Engineering
Trinity College
Hartford, CT, 06106, United States
clayton.byers@trincoll.edu

Kelly Y. Huang
Mechanical and Aerospace Engineering
University of Houston
Houston, TX, 77204, United States
yhuang68@uh.edu

ABSTRACT

Active grids offer direct control over the spectral content of wind tunnel turbulence through the choice of actuation parameters. This work examines the nonlinear frequency interactions produced by an active grid built from off-the-shelf components, driven simultaneously at two flapping frequencies of 3 Hz and 5 Hz with a 25-degree angular amplitude at a freestream velocity of 8 m/s. Hot-wire anemometry measurements were taken at 14 streamwise locations spanning from 20 to 280 inches downstream of the grid. The power spectra show discrete peaks not only at the two forcing frequencies but also at their sum, difference, and harmonic combinations, confirming active nonlinear triadic interactions in the flow. The bicoherence identifies statistically significant quadratic phase coupling at the forcing frequencies and their triadic combinations, with measurable coupling persisting to the farthest measurement location. The biphase, computed with a statistical significance mask based on the number of ensemble averages, reveals a coexistence of forward and reverse energy cascade events in the sub-forcing-frequency range, consistent with theoretical predictions for externally forced turbulent flows. The spatial evolution from near-field to far-field shows a clear transition from organized, broadband phase coupling in the near field to a state of decay in the far field, where statistically significant coupling is confined to the directly forced modes.

INTRODUCTION

Active grids generate turbulence at Reynolds numbers far beyond the reach of passive grids by mechanically agitating the flow through an array of rotating paddle rods (Hideharu, 1991; Mydlarski & Warhaft, 1996). When operated under a structured periodic protocol, the paddle motions inject energy at specific frequencies, and two simultaneous forcing frequencies f_1 and f_2 produce spectral peaks not only at f_1 and f_2 but also at their sum, difference, and harmonic combinations. These combination tones are the spectral signature of nonlinear triadic interactions (Waleffe, 1992). The power spectrum alone cannot determine whether these peaks arise from genuine quadratic phase coupling or from the simple coexistence of unrelated energy at those frequencies (Kim & Powers, 1979). The level of quadratic phase coupling can be determined from the bispectrum, a third-order complex-valued spectrum that retains phase relationships across frequency pairs (Kim & Powers, 1979). Its normalized form, the bicoherence, quantifies the fraction of energy at the sum of two frequency attributable to quadratic phase coupling, and the biphase indicates the direction of the associated energy cascade (Cui & Jacobi, 2021; Waleffe, 1992). Waleffe (1992) showed through helical mode decomposition that all triadic interactions reduce to two classes: Class F interactions draw energy from the largest scale and produce a forward cascade, while Class R interactions draw from the middle scale and constitute a reverse cascade. This framework provides the theoretical basis for interpreting the coexistence of forward and reverse cascade events in externally forced turbulence. Most bispectral analyses of turbulent flows have been conducted at a single streamwise location (Cui & Jacobi, 2021). The spatial development of triadic coupling along the streamwise direction has not been examined through bispectral analysis. The present work applies bispectral analysis to free-stream turbulence generated by an active grid with simultaneous sinusoidal forcing at two harmonically distinct frequencies. Three main findings are reported: the two forcing frequencies decay at fundamentally different rates, with the lower-frequency mode maintaining strong self-coupling throughout the domain; the difference-frequency triad is the most persistent interaction, suggesting the lower mode is sustained through a nonlinear feeding pathway; and secondary triadic interactions develop over a finite downstream distance before decaying, a feature that single-location measurements cannot resolve.

EXPERIMENTAL SETUP

All experiments were conducted in the closed-loop wind tunnel at the University of Houston. The rectangular test section measures 42×66 in^2 in cross-section. A freestream velocity of $U_\infty = 8$ m/s was maintained for all measurements, giving a mesh Reynolds number $Re_M = U_\infty M/\nu \approx 1.45 \times 10^4$ based on the paddle size $M = 5$ in.

Flow perturbations were introduced using a custom active grid installed at the test section inlet. The grid consists of 136 square paddles of side length M, each independently actuated by a servo motor driven through an Arduino-based control system. The outermost ring of paddles was fixed in the fully open position to isolate the centrally driven paddles from wall-adjacent boundary effects.

The active paddles were arranged in a spatial checkerboard pattern, with adjacent paddles assigned to different actuation signals. One subset followed a sinusoidal motion at $f_1 = 3$ Hz and the other at $f_2 = 5$ Hz, both at an angular amplitude of $\pm 25^\circ$. The two frequencies are not harmonically related, so their triadic products — the sum $f_1 + f_2 = 8$ Hz, the difference $f_2 - f_1 = 2$ Hz, and higher-order combinations — are spectrally distinct from the self-coupling harmonics of either frequency. Both signals were generated from a shared timing reference, fixing the relative phase between the two forcing frequencies across each experimental run.

Streamwise velocity measurements were acquired using a Dantec Dynamics 55P11 single-wire hot-wire probe in constant-temperature anemometry mode. The signal was sampled at 10 kHz, and 1200 s of continuous data were recorded at each location. This duration provides sufficient ensemble averaging for converged bispectral estimates and suppresses spurious phase coupling below the statistical significance threshold. The probe was traversed along the tunnel centerline to 14 streamwise locations between $x/M = 4$ and $x/M = 56$, spanning the near-grid region through the far field where the organized forcing structure has decayed into a broader turbulent background.

ANALYSIS METHODS

The quadratic nonlinearity of the Navier–Stokes equations couples Fourier modes in triads satisfying $f_3 = f_1 + f_2$. These interactions produce systematic phase relationships essential to the formation of the energy cascade (Kim & Powers, 1979; Waleffe, 1992; Duvvuri & McKeon, 2016; Wang *et al.*, 2024). The conventional power spectrum $P(f) = \langle |X(f)|^2 \rangle$ identifies the distribution of energy across frequencies but discards all phase information. Phase-coupled dynamical states are therefore invisible in power spectra alone, even when the underlying coupling is strong (Lii *et al.*, 1976; George *et al.*, 2017; Lyu *et al.*, 2020). To quantify these interactions directly, we employ the bispectrum of the streamwise velocity fluctuation $u(t)$, defined as:

$$B(f_1, f_2) = \langle X(f_1), X(f_2), X^*(f_1 + f_2) \rangle \tag{1}$$

where $X(f)$ is the Fourier transform of a windowed segment of the streamwise velocity and the asterisk denotes complex conjugation (Kim & Powers, 1979). As the third-order analog of the power spectrum, $B(f_1, f_2)$ is complex-valued and retains phase relationships; its real part, when integrated, recovers the velocity skewness (Lii *et al.*, 1976; Van Atta, 1979; Midya *et al.*, 2022). Significant triadic coupling is present when the phase sum $\phi(f_1) + \phi(f_2) - \phi(f_3)$ is non-random across ensembles (Haubrich, 1965). To isolate the coupling strength from the local energy levels, we utilize the bicoherence $b(f_1, f_2)$:

$$b(f_1, f_2) = \frac{|B(f_1, f_2)|}{\sqrt{P(f_1)P(f_2)P(f_1 + f_2)}} \tag{2}$$

which represents the fraction of energy at f_3 attributable to quadratic phase coupling (QPC) between f_1 and f_2 (Greb & Rusbridge, 1988; Cui & Jacobi, 2021). Unlike filtering-based approaches that can impose artificial phase relationships (Jacobi & McKeon, 2013; Baars *et al.*, 2015; Kovach *et al.*, 2018), the bicoherence operates directly in Fourier space without requiring arbitrary bandwidth selection (Zandvoort & Nolte, 2021).While b quantifies coupling intensity, the direction of the associated energy transfer is carried by the biphase:

$$\beta(f_1, f_2) = \tan^{-1}\left(\frac{\mathrm{Im}\{B\}}{\mathrm{Re}\{B\}}\right) \tag{3}$$

In the ensemble limit, β converges to the phase delay ϕ_D between the high-frequency component and the lower-frequency pair that produces it (Jacobi & McKeon, 2013; Duvvuri & McKeon, 2015). The sign convention depends on the measurement domain. Theoretical analyses formulated in wavenumber space assign $\beta \in (0, \pi)$ to the forward cascade; for time-domain signals such as single-point hot-wire measurements, this assignment is reversed (Cui & Jacobi, 2021). For the present measurements, $\beta \in (-\pi, 0)$ indicates a forward energy cascade from lower to higher frequencies, and $\beta \in (0, \pi)$ indicates a reverse cascade. This classification aligns with the broader framework of cascade directions in both homogeneous and active turbulence (Alexakis & Biferale, 2018; Słomka *et al.*, 2018). For the present analysis, records of 1200 seconds sampled at 10 kHz were divided into 20 second segments with 90% overlap. This yields $N_{\text{seg}} = 591$ averages and a frequency resolution of $\Delta f = 0.05$ Hz, ensuring that grid-forcing frequencies and their triads fall on distinct bins. To avoid interpreting random phase fluctuations, we apply a significance threshold $b_{\text{sig}} = \sqrt{2/N_{\text{seg}}} \approx 0.058$ (Haubrich, 1965; Elgar & Sebert, 1989). Bicoherence values below b_{sig} are retained in the plots but set to zero, as they are indistinguishable from sampling noise. The biphase is masked entirely at those frequency pairs, since a phase estimate without significant coupling carries no physical meaning (Elgar & Sebert, 1989; Cui & Jacobi, 2021). The resulting estimates provide a stable representation of the triadic architecture of the flow.

RESULTS

Figure 1 compares power spectra at $x/M = 52$ under active and passive-grid conditions. The passive-grid spectrum shows broadband turbulent decay with no discrete spectral features. Under active-grid forcing, the strongest peaks appear at the forcing frequencies of 3 Hz and 5 Hz, with combination tones at 2 Hz and 8 Hz, and harmonics at 6 Hz and 10 Hz also present. The spectral content above approximately 20 Hz decays onto the passive-grid curve, confirming that the deterministic forcing does not alter the high-frequency turbulent dynamics. The presence of combination tones is consistent with triadic frequency interactions, but the power spectrum cannot distinguish genuine quadratic phase coupling from the statistical coexistence of energy at those frequencies (Kim & Powers, 1979). Figure 2 shows power spectra at $x/M = 4$, 28, and 56. The 3 Hz and 5 Hz peaks persist at all three locations, confirming that the forced modes remain energetically active throughout the measurement domain. Near the grid exit, a low-frequency peak at 1 Hz is visible, consistent with the indirect combination $3 - (5 - 3) = 1$ Hz. This feature decays with downstream distance and is absent in the far field.

Figure 3 shows bicoherence maps at $x/M = 4$, 28, and 56, masked for statistical significance (Elgar & Sebert, 1989). At

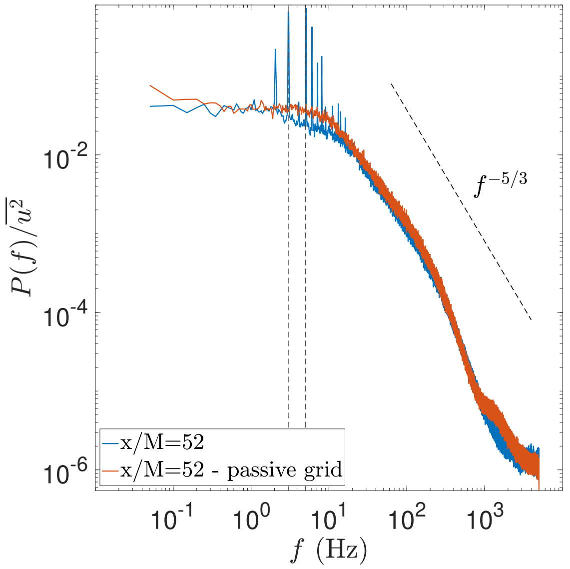

Figure 1: Power spectral density at $x/M = 52$ under passive-grid (red) and active-grid (blue) forcing conditions. The dashed vertical lines mark the forcing frequencies (3 Hz and 5 Hz).

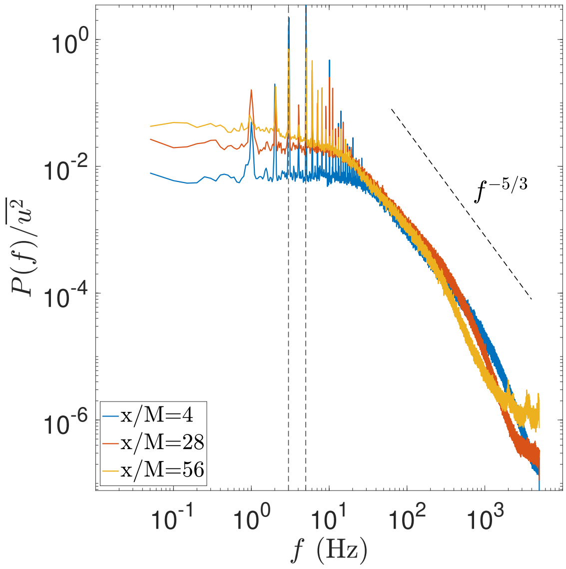

Figure 2: Power spectral density at $x/M = 4$, 28, and 56, corresponding to streamwise distances of 20, 140, and 280 inches from the grid. The dashed vertical lines mark the forcing frequencies, with a theoretical $-5/3$ slope shown for reference.

$x/M = 4$, bicoherence is elevated broadly across the frequency plane, reflecting transient phase relationships in the near-field grid wake. By $x/M = 28$, the broadband background has decayed and bicoherence concentrates into discrete peaks. At $x/M = 56$, coupling is confined to a small number of well-defined frequency pairs, all corresponding to combinations of 3 Hz and 5 Hz and their sum and difference tones. This spatial transition from broadband to discrete coupling is consistent with the progressive decay of grid-generated turbulence and the emergence of scale-selective nonlinear interactions (Duvvuri & McKeon, 2015, 2016).

Figure 4 shows biphase maps at the same three locations as Fig. 3, retaining values only where the bicoherence is statistically significant (Elgar & Sebert, 1989). Following Cui & Jacobi (2021), a biphase in $(-\pi, 0)$ indicates a forward energy cascade and a biphase in $(0, \pi)$ indicates a reverse cascade. At $x/M = 4$, the 3 Hz line is predominantly negative while the 5 Hz line shows a mixed distribution. By $x/M = 56$, both forcing-frequency lines are predominantly negative, indicating a net forward energy transfer in the far field.

The $(3,3)$ biphase is negative at every location, indicating a consistent forward cascade from 3 Hz to 6 Hz throughout the domain. The $(5,5)$ biphase shows positive values in the near field, indicating a transient reverse cascade during the period of its strongest coupling, before transitioning to negative values further downstream. The $(3,5)$ triad undergoes a sign reversal between $x/M = 12$ and $x/M = 16$, marking a shift from forward to reverse and back to forward cascade for the primary sum-frequency interaction. The $(2,3)$ biphase remains near $\pm\pi$ at all locations, indicating that the $2+3 = 5$ Hz interaction maintains a near-standing phase relationship with no systematic preferential cascade direction. This is consistent with the high and persistent bicoherence of this pair: the 5 Hz mode is continuously regenerated through the difference-frequency pathway without directional energy preference. Together, the two forcing frequencies generate qualitatively distinct interaction networks. The 3 Hz mode drives persistent, self-reinforcing triadic coupling throughout the full domain. The 5 Hz mode generates stronger initial coupling but loses phase coherence faster. The $(2,3)$ difference-frequency triad acts as the primary energy conduit between the two forcing modes, sustaining the 5 Hz mode over distances at which its own self-coupling has already decayed substantially. Additionally, combinations of frequencies that add to 3 and 5 Hz, seen as the diagonals in Fig. 4, tend to have positive phase, indicating that these two forcing frequencies are continually sending energy in a reverse cascade to lower frequencies.

Three distinct evolutionary regimes are visible in Figure 5, which shows the downstream evolution of bicoherence and biphase at the six target pairs from $x/M = 4$ to $x/M = 56$. The $(3,3)$ and $(2,3)$ triads maintain bicoherence above 0.74 and 0.68, respectively, at all downstream locations, with no systematic decay. Their persistence identifies the 3 Hz mode as the anchor of the nonlinear interaction network. The $(5,5)$ and $(2,5)$ triads decay monotonically with downstream distance. The $(5,5)$ bicoherence falls from 0.91 at $x/M = 4$ to 0.10 by $x/M = 44$. Under Taylor's frozen-field hypothesis (Taylor, 1938), a temporal frequency f corresponds to a spatial wavelength $\lambda = u_\infty/f$ at a fixed convection velocity. Higher-frequency modes therefore represent shorter spatial scales, which are expected to lose phase coherence over shorter streamwise distances. This provides a physical basis for the observed asymmetry between the 3 Hz and 5 Hz self-coupling persistence. The $(3,8)$ triad exhibits a third behavior: it is negligible at $x/M = 4$, grows to a peak of 0.774 near $x/M = 16$, and decays below the significance threshold beyond $x/M = 32$. This secondary interaction requires the 8 Hz mode to first be produced by the primary $3+5 = 8$ Hz coupling before it can participate in a further interaction with the 3 Hz mode, and its decay coincides with the decay of the $(5,5)$ bicoherence. This three-stage behavior — absence, growth, decay — provides direct evidence that the nonlinear interaction network is not fully established immediately downstream of the grid. Single-location measurements would observe only the intermediate state and could not distinguish between a developing and a decaying secondary interaction.

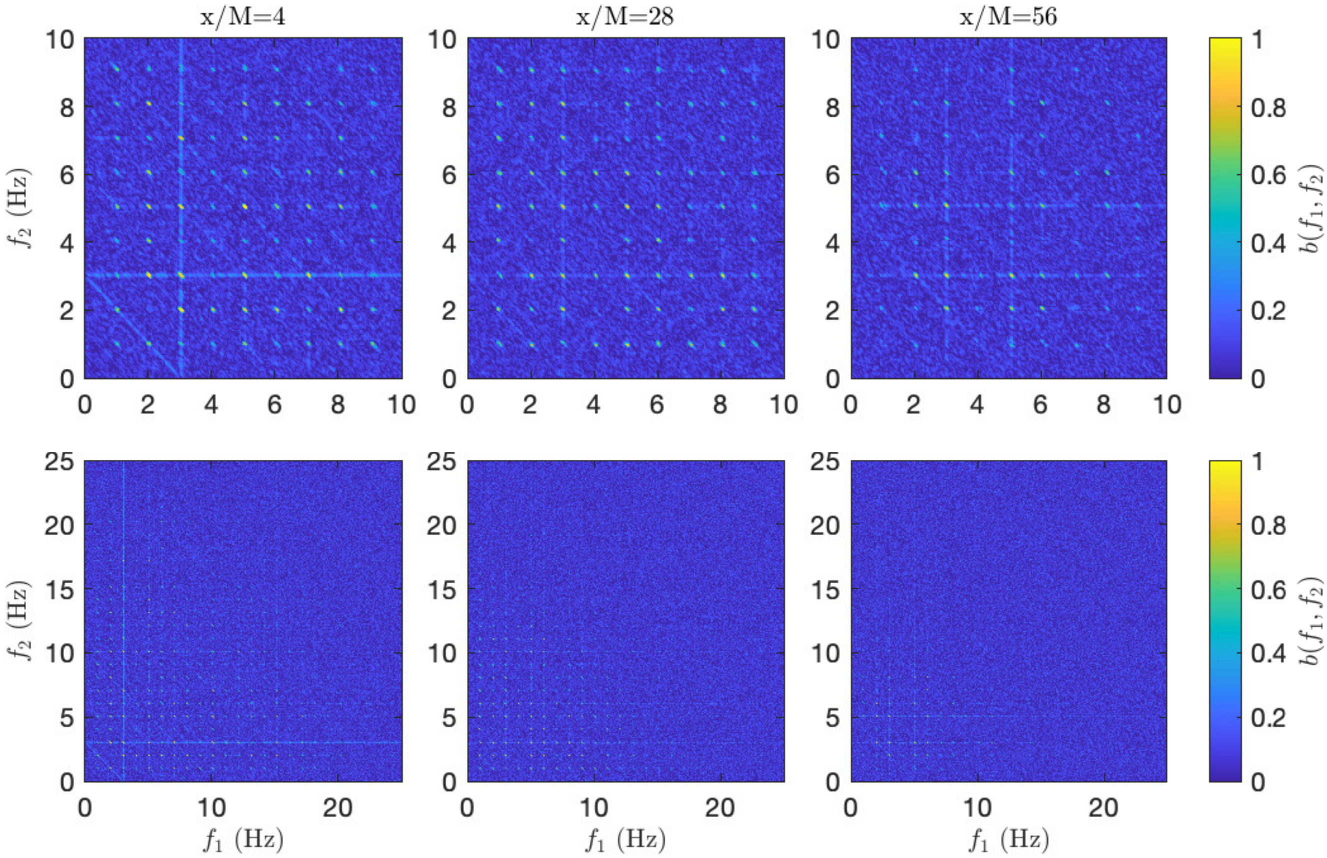

Figure 3: Two-dimensional bicoherence maps $b(f_1, f_2)$ at $x/M = 4$, 28, and 56 from the grid. Top row: zoomed view for $f_1, f_2 \leq 10$ Hz. Bottom row: full frequency range.

The coexistence of forward and reverse cascade events observed here is consistent with the Waleffe (1992) classification of triadic interactions into Class F and Class R. Class F interactions extract energy from the largest scale in a triad and transfer it to smaller scales; Class R interactions draw from the middle scale and can feed energy back to larger scales. The near-field biphase maps, where both positive and negative values appear across the forced frequency lines, suggest that both classes are active simultaneously in the early stages of the flow. The convergence toward predominantly negative biphase values in the far field indicates that Class F interactions become dominant as the organized forcing structure decays. The (2,3) triad is a notable exception: its biphase near $\pm\pi$ at all locations suggests a balance between the two classes, consistent with its role as a regeneration pathway rather than a net energy conduit in one direction. The biphase panel of Figure 5 adds cascade direction to each regime. The $(3,3)$ biphase is negative at every location, confirming a consistent forward cascade from 3 Hz to 6 Hz throughout the domain. The $(5,5)$ biphase is positive at $x/M = 8$ and 12, marking a transient reverse cascade during the period of its strongest coupling, before settling to negative values further downstream. The $(3,5)$ triad undergoes a sign reversal between $x/M = 12$ and 16, then returns to consistently negative values from $x/M = 20$ onward. The $(3,8)$ biphase begins positive at $x/M = 4$ and transitions to negative from $x/M = 8$ onward, developing a forward cascade direction in parallel with its growing bicoherence, before dropping below significance at large x/M.

CONCLUSION

This study characterized the nonlinear triadic interactions produced by an active grid under simultaneous dual-frequency sinusoidal forcing at 3 Hz and 5 Hz, using bispectral analysis at 14 streamwise locations spanning $x/M = 4$ to $x/M = 56$. Three findings emerged from the spatial evolution of the bicoherence and biphase maps.

First, the two forcing frequencies generate qualitatively distinct interaction networks that decay at fundamentally different rates. The 3 Hz mode maintains strong self-coupling and persistent bicoherence throughout the entire measurement domain. The 5 Hz mode produces higher initial coupling near the grid but loses phase coherence monotonically with downstream distance. This asymmetry is consistent with the expectation that higher-frequency modes, corresponding to shorter spatial scales under Taylor's frozen-field hypothesis (Taylor, 1938), lose phase coherence over shorter streamwise distances at a fixed convection velocity.

Second, the difference-frequency triad at $(2,3)$ Hz is the most persistent nonlinear interaction in the flow. Its bicoherence remains elevated at all downstream locations and its biphase stays near $\pm\pi$, indicating that the 3 Hz and 2 Hz modes continuously regenerate the 5 Hz mode through a quadratic sum interaction with no strong directional preference. This pathway sustains the 5 Hz mode over distances at which its own self-coupling has already decayed substantially, identifying difference-frequency regeneration as the dominant interscale energy conduit in this forced configuration. Third, the $(3,8)$ Hz secondary triad follows a three-stage evolution not resolvable from measurements at a single downstream lo-

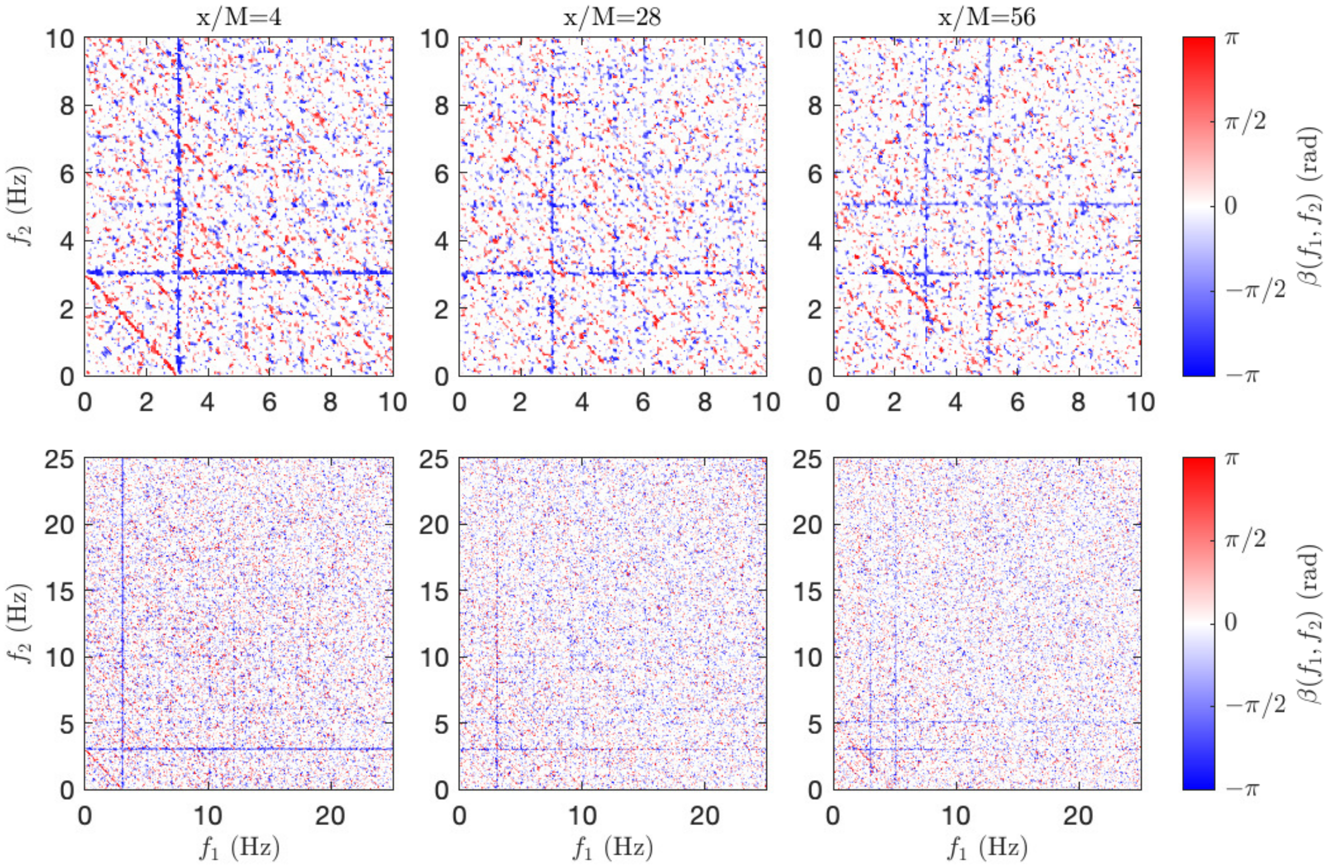

Figure 4: Two-dimensional biphase maps $\beta(f_1, f_2)$ at $x/M = 4$, 28, and 56 from the grid. Top row: zoomed view for $f_1, f_2 \leq 10$ Hz. Bottom row: full frequency range. Values are shown only where the bicoherence is statistically significant.

cation. It is negligible near the grid, grows to a peak near $x/M = 16$ once sufficient 8 Hz energy has been produced by the primary $3+5$ Hz coupling, and decays beyond $x/M = 32$ in parallel with the decay of $(5,5)$ self-coupling. This behavior confirms that secondary triadic interactions in forced turbulence are feedforward: they require the prior establishment of primary product modes before they can emerge (Waleffe, 1992; Duvvuri & McKeon, 2015). The biphase analysis revealed a coexistence of forward and reverse energy cascade events, consistent with the theoretical expectation for externally forced flows (Waleffe, 1992; Cui & Jacobi, 2021). In the near field, both forcing-frequency lines show mixed cascade directions. By $x/M = 56$, both converge toward predominantly negative biphase values, indicating a net forward energy transfer consistent with a flow in which the organized forcing structure has largely decayed into broadband turbulence. The transition from broadband phase coupling in the near field to discrete, forcing-frequency-anchored coupling in the far field provides a clear picture of how deterministic injection evolves toward unforced turbulent decay (Kang *et al.*, 2003; Hearst & Lavoie, 2015). These results demonstrate that the active grid is not simply a broadband turbulence generator when operated under deterministic dual-frequency forcing, and that any injected structure may continue to persist through QPC feedback of energy. The nonlinear interaction structure is reproducible, frequency-selective, and spatially resolved through bispectral analysis without any arbitrary filtering. The approach generalizes to other forcing configurations and offers a direct means of characterizing energy injection mechanisms in any wind tunnel facility employing structured active grid protocols.

REFERENCES

Alexakis, A. & Biferale, L. 2018 Cascades and transitions in turbulent flows. *Physics Reports* **767-769**, 1–101, cascades and transitions in turbulent flows.

Baars, W. J., Talluru, K. M., Hutchins, N. & Marusic, I. 2015 Wavelet analysis of wall turbulence to study large-scale modulation of small scales. *Experiments in Fluids* **56**, 188.

Cui, G & Jacobi, I 2021 Biphase as a diagnostic for scale interactions in wall-bounded turbulence. *Physical Review Fluids* **6** (1), 014604.

Duvvuri, Subrahmanyam & McKeon, Beverley 2015 Triadic scale interactions in a turbulent boundary layer. *Journal of Fluid Mechanics* **767**, R4.

Duvvuri, Subrahmanyam & McKeon, Beverley 2016 Nonlinear interactions isolated through scale synthesis in experimental wall turbulence. *Phys. Rev. Fluids* **1**, 032401.

Elgar, Steve & Sebert, Gloria 1989 Statistics of bicoherence and biphase. *Journal of Geophysical Research: Oceans* **94** (C8), 10993–10998.

George, Sandip V., Ambika, G. & Misra, R. 2017 Detecting dynamical states from noisy time series using bicoherence. *Nonlinear Dynamics* **89** (1), 465–479.

Greb, U & Rusbridge, M G 1988 The interpretation of the bispectrum and bicoherence for non-linear interactions of continuous spectra. *Plasma Physics and Controlled Fusion* **30** (5), 537.

Haubrich, Richard A. 1965 Earth noise, 5 to 500 millicycles per second: 1. spectral stationarity, normality, and nonlinearity. *Journal of Geophysical Research* **70**, 1415–1427.

Hearst, R. J. & Lavoie, P. 2015 The effect of active grid initial

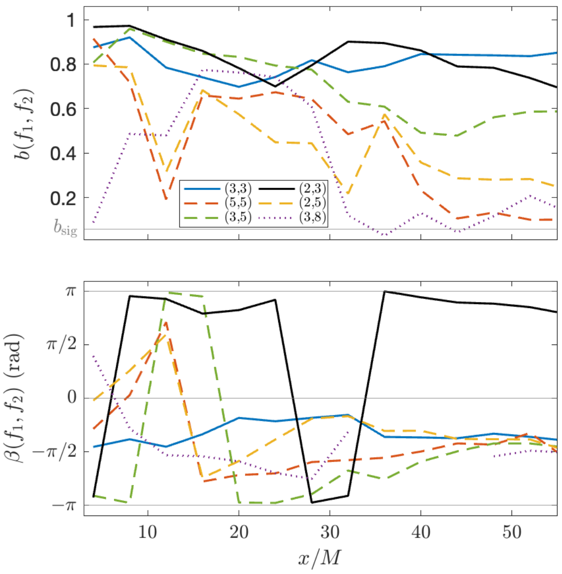

Figure 5: Downstream evolution of bicoherence (top) and biphase (bottom) at six target frequency pairs from $x/M = 4$ to $x/M = 56$. Solid lines: persistently coupled pairs $(2,3)$ and $(3,3)$. Dashed lines: decaying pairs $(5,5)$, $(2,5)$, and $(3,5)$. Dotted line: secondary triad $(3,8)$. The horizontal grey line in the top panel marks the statistical significance threshold b_{sig}. Biphase values are omitted where the bicoherence falls below b_{sig}. Grey reference lines at $\beta = 0$ and $\beta = \pm\pi$ mark the forward/reverse cascade boundary and the near-standing-wave limit, respectively.

conditions on high reynolds number turbulence. *Exp. Fluids* **56** (10), 185.

Hideharu, Makita 1991 Realization of a large-scale turbulence field in a small wind tunnel. *Fluid Dynamics Research* **8** (1), 53–64.

Jacobi, I. & McKeon, B. J. 2013 Phase relationships between large and small scales in the turbulent boundary layer. *Exp. Fluids* **54** (3).

Kang, Hyung Suk, Chester, Stuart & Meneveau, Charles 2003 Decaying turbulence in an active-grid-generated flow and comparisons with large-eddy simulation. *Journal of Fluid Mechanics* **480**, 129–160.

Kim, Young C. & Powers, Edward J. 1979 Digital bispectral analysis and its applications to nonlinear wave interactions. *IEEE Transactions on Plasma Science* **7** (2), 120–131.

Kovach, Christopher K., Oya, Hiroyuki & Kawasaki, Hiroto 2018 The bispectrum and its relationship to phase-amplitude coupling. *NeuroImage* **173**, 518–539.

Lii, K. S., Rosenblatt, M. & Atta, C. Van 1976 Bispectral measurements in turbulence. *Journal of Fluid Mechanics* **77** (1), 45–62.

Lyu, Wan, Gu, Wen, Wu, Xi, Yang, Hongyu, Jiang, Chen & Xu, Shanshan 2020 Correlation analysis between forced oscillation modes caused by wind power. *Journal of Physics: Conference Series* **1639** (1), 012062.

Midya, S., Thomas, F. & Gordeyev, S. 2022 On the spectral decomposition of skewness in canonical and actuated turbulent boundary layers. In *Proceedings of the 12th International Symposium on Turbulence and Shear Flow Phenomena (TSFP12)*. Osaka, Japan.

Mydlarski, Laurent & Warhaft, Z. 1996 On the onset of high reynolds number grid-generated wind tunnel turbulence. *JFM* **320**, 331–368.

Słomka, Jonasz, Suwara, Piotr & Dunkel, Jörn 2018 The nature of triad interactions in active turbulence. *Journal of Fluid Mechanics* **841**, 702–731.

Taylor, G. I. 1938 The spectrum of turbulence. *Proceedings of the Royal Society of London. A. Mathematical and Physical Sciences* **164** (919), 476–490.

Van Atta, C. W. 1979 Inertial range bispectra in turbulence. *The Physics of Fluids* **22** (8), 1440–1442.

Waleffe, Fabian 1992 The nature of triad interactions in homogeneous turbulence. *Physics of Fluids A: Fluid Dynamics* **4** (2), 350–363.

Wang, Chuhan, Fang, Le, Wang, Zhan & Xu, Chunxiao 2024 Role of fourier phase dynamics in decaying turbulence. *Phys. Rev. Fluids* **9**, 114603.

Zandvoort, Coen S. & Nolte, Guido 2021 Defining the filter parameters for phase-amplitude coupling from a bispectral point of view. *Journal of Neuroscience Methods* **350**, 109032.